Directional spectral reflectivity measurements of a carbon fibre reinforced composite up to 450 °C

Violaine Le Louët, Benoit Rousseau, Steven Le Corre, Nicolas Boyard, Xavier Tardif, Jérôme Delmas, Didier Delaunay

Directional spectral reflectivity measurements of a carbon fibre reinforced composite up to 450°C.

Violaine Le Louët[a,b], Benoit Rousseau[b*], Steven Le Corre[b], Nicolas Boyard[b], Xavier Tardif [a], Jérôme Delmas [b], Didier Delaunay [b].

[a] Institut de Recherche Technologique Jules Verne, Chemin du Chaffault, 44340 Bouguenais, France

[b] Laboratoire de Thermocinétiques de Nantes, UMR CNRS 6607, Université de Nantes, Rue Christian Pauc, 44306 Nantes, France

Keywords: Radiative properties, Spectrometer, controlled-temperature cell, carbon fibre reinforced composite

Abstract:

A quantitative study of the bi-directional reflectivity of a carbon/poly-ether-ether-ketone (PEEK) based composite is performed at room temperature using a Fourier Transform Infra-Red Bruker 80v spectrometer (0.6-25 µm i.e. 400-15000 cm^{-1}) with angles of incidence and collection ranging from 11 to 83° and by varying fibre orientation. Then, a home-made compact cell, based on a customized resistive heater, is adapted to the sample compartment of the spectrometer for measuring the temperature dependency of the normal reflectivity of the composite sample from 20 to 450°C. A complete validation of the thermal performances of the cell is thus presented to support the interpretation of the previous reflectivity measurements. The respective contributions of the carbon fibrous reinforcement and of the PEEK matrix on the reflective behaviour up to 450°C is finally discussed. Temperature is shown to play a minor role on the optical properties of the tested materials, thus indicating a predominant role of the carbon fibres. Conversely, the room temperature angular study shows the high importance of the beam incident angle with respect to fibres orientation and enables to characterize this strongly anisotropic reflective behaviour.

*Corresponding author. Email address: benoit.rousseau@univ-nantes.fr

Summary

*Corresponding author. Email address: benoit.rousseau@univ-nantes.fr

I. Introduction

Thanks to their advantageous strength to weight ratio, Carbon Fibre Reinforced Polymer composites (CRFP) have become an alternative to metals and associated alloys in numerous applications, ranging from sporting goods to aircraft structures. Nowadays, the manufacturing of aeronautical structural parts is very often achieved by the automated lay-up of successive composite tapes one upon another [1]. In this process, the composite layers are made of unidirectional carbon fibres pre-impregnated by a thermoset matrix. At each deposition pass, the incoming tape is heated up together with the substrate, and brought into contact with the substrate by a conformation roller that applies a certain pressure. The newly formed laminate surface can then cool, generally under natural conditions, before the next pass. According to the deposition shape and complexity the process name varies (Tape Laying (TP), Fibre Placement (FP) or Filament Winding (FW)) but they are all bases upon the same physical phenomena: the adhesion of the tapes by the bonding of the polymeric matrices at their surfaces and the consolidation of the laminate.

The development of high performance semi-crystalline thermoplastic polymers such as poly-ether-ether-ketone (PEEK) led to their increasing use as matrix in the pre-impregnated tapes instead of thermoset resins. In this case, thanks to the ability of the crystalline parts to melt, the bonding at the interface is achieved by the welding of the polymer-rich tapes surfaces by intimate contact then molecular inter-diffusion [2]. Thermoplastic composites then offer the possibility of a faster out-of-autoclave process [3] as well as post-manufacturing reparation and even recyclability of the parts, since the melting is an easily controlled and reversible transformation.

In parallel to the development of advanced thermoplastic materials, near infrared heat sources are now being preferred to the traditional hot gas or air torches thanks to major technological developments. Those compact devices deliver, *via* an optical fibre, high uniform heat fluxes over surfaces up to 200×200 mm^2, with a short response time (order of the ms) [4] . Thanks to the feeble clutter of the light cable in the Automated Fibre Placement (AFP) process, the laser is generally inclined close to the substrate surface so as to heat the deposited tape and the substrate as close as possible to the contact point.

*Corresponding author. Email address: benoit.rousseau@univ-nantes.fr

In order to optimize the energy efficiency of the laser assisted processes such as AFP, the thermal radiative properties of the materials involved is required. The process can be optimized if the amount of laser radiation absorbed, transmitted and reflected by the material is accurately known according to the beam wavelength λ, the temperature T of the irradiated area, the incident direction and the scattered light angles.

Besides, it is known that CFRP have a strong back-scattering power due to the presence of cylindrical fibres [6] and simple specular reflection assumptions fail to correctly model the surface/laser interaction [7,8]. The diffusive behaviour is influenced by the angle of incidence and by the fibres orientation. To illustrate this behaviour, directional hemispherical reflectivity measurements have been performed at room temperature with the beam aligned to the fibre directions at 0.5, 1, 1.5 and 2 µm on a carbon/PEEK composite by varying the incident angles between 10 and 80° [5]. It was found that the reflected flux rises from 10% to 60% when the beam is shifted from normal incidence to a grazing one. Moreover, similarly to the pioneering experiment carried out by Grouve [8], the same authors qualitatively observed that the scattering profile of the composite surface is highly dependent of the angle, ϕ, between the axis of the fibre and the axis of the laser. In Hohmann et al. [6], total directional reflections measurements were performed at 500 nm with integrating spheres on carbon fibre laminates, one where the polymer matrix at the surface was removed by laser processing, and the other one with the polymer layer at the surface. Results showed that the normal total reflectivity was 2% higher for the latter sample. The authors explained this reflectivity increasing by the fact that the matrix alone has a higher refractive index so that a little less light is absorbed. Eventually, in parallel to experimental studies on composite materials, optical models based on Ray Tracing [5] or Maxwell Equations [6] were developed. Nevertheless, whatever the primary assumptions, they all required the accurate knowledge of the optical indexes n and k of the material that can only be obtained with fine optical measurements.

From this point, it appears that still few studies dealing with the high temperature optical properties (up to 450°C) of CFRP have been carried out. Nevertheless, it is expected the radiative properties of CFRP can evolve, especially when the PEEK matrix melts (around

*Corresponding author. Email address: benoit.rousseau@univ-nantes.fr

343°C) or due to thermal degradations at higher temperatures. Above 350°C the phenomena involved are oxidation and crosslinking of the polymers chains. They are speeded up under oxygen [9,10] and can start just above the melting point, depending also on the holding times.

The knowledge of the effects played by the temperature on the radiative properties are therefore crucial for bringing accurate data in order to run thermal modelling works. One can note the preliminary work of Grouve [8], who used a crude resistive heater placed under a carbon/(Polyphenylene sulphide) PPS composite sample in order to perform reflectivity measurement only at 1080 nm between 25 and 350°C. The author qualitatively observed negligible variations but little information was given on the performances and thermal homogeneity of the heating apparatus. On the other hand, limiting the campaign of radiative measurements only at the wavelength of the impinging laser reduces the exactness of the thermal modelling since hot CFRP tapes are also likely to emit thermal radiation in the infrared spectral range where Plank's law predicts significant emission around 450°C. Therefore, with the goal of providing accurate high temperature spectral quantities, we propose here to develop a compact cell able to investigate the reflective behaviour of CFRP for a spectral range going from 1 to 20 µm and a temperature ranging from 20 up to 450°C. Let us note that several set-ups, based on small furnaces [11,12] or ceramic plates [13] have been developed but none description and/or validation of their thermal performances can be easily found. At higher temperatures (up to 2500°C), directional spectral emissivity measurements [14–22] are available but few are today able to cover, with accuracy, the low temperature range (from room temperature up to 450°C). For these later devices, if materials are optically thick and optically smooth, measuring their emissivities comes down to investigate, indirectly, their reflectivities.

In order to refine the analysis of the reflective behaviour of a carbon/PEEK composite, the following study aims firstly at quantifying the reflected intensities along the diffusion profile of an incident beam through a Bruker 80v IRTF spectrometer equipped with a directional measurement unit. The spectral range covered by the spectrometer goes from 0.66 up to 25 µm i.e. from 400 to 15000 cm^{-1} and the bidirectional study can be performed for incident angles ranging from 15 to 83°C. Secondly, an original compact cell, based on

*Corresponding author. Email address: benoit.rousseau@univ-nantes.fr

a customized resistive heater, is proposed in this work to investigate the evolution of the normal reflectivity with temperature. The cell is inserted in the sample compartment of a Bruker 80v Fourier Transform Infrared (FTIR) spectrometer and allows performing measurements on opaque materials from 20 up to 600°C. After the determination of the thermal and optical performances of the developed heating unit, the results obtained on the carbon/PEEK composite are presented. Finally the role of each phase of the composite sample on its global radiative behaviour will be discussed.

2. Experimental procedure

2.1. Definitions of the main radiative quantities

Before describing the experimental set-up used to perform the measurements, let us define the main radiative quantities of interest in this study. Figure 1 shows how the incident beam can interact with the surface of the composite. With respect to the normal axis of the plane bearing the CFRP sample, let us define θ_i the polar incident angle and the azimuthal angle ϕ_i , which is the deviation angle with the main direction of the unidirectional fibres. The bi-directional reflectivity function BRDF, $f_\lambda(\theta_r, \phi_r, \theta_i, \phi_i, T)$, is defined by:

$$f_\lambda(\theta_r, \phi_r, \theta_i, \phi_i, T) = \frac{I_{\lambda,r}(\theta_r, \phi_r, \theta_i, \phi_i, T)}{I_\lambda(\theta_i, \phi_i, T) cos\theta_i d\Omega_i} \quad \text{Eq. 1}$$

where, $I_{\lambda,r}(\theta_r, \phi_r, \theta_i, \phi_i, T)$ is the reflected spectral intensity in direction (θ_r, ϕ_r) due to the irradiance $I_\lambda(\theta_i, \phi_i, T) cos\theta_i d\Omega_i$ in the incident direction (θ_i, ϕ_i). Here T stands for the temperature and $d\Omega_i$ is the elementary solid angle around direction (θ_i, ϕ_i). The bi-directional reflectivity is given by:

$$\rho_\lambda(\theta_r, \phi_r, \theta_i, \phi_i, T) = f_\lambda(\theta_r, \phi_r, \theta_i, \phi_i, T)\cos(\theta_r) d\Omega_r \quad \text{Eq. 2}$$

At last, the spectral directional hemispherical reflectivity, $\hat{\rho}_\lambda(\theta_i, \phi_i, T)$ is given by:

$$\hat{\rho}_\lambda(\theta_i, \phi_i, T) = \int_{2\pi} f_\lambda(\theta_r, \phi_r, \theta_i, \phi_i, T)\, cos\, \theta_r d\Omega_r \quad \text{Eq. 3}$$

*Corresponding author. Email address: benoit.rousseau@univ-nantes.fr

where $d\Omega_r$ is the solid angle around (θ_r, ϕ_r).

For opaque materials at thermal equilibrium such as CRFP, in the infrared range, the directional absorptivity $a_\lambda(\theta_i, \phi_i, T)$ is linked to the directional emissivity $\varepsilon_\lambda(\theta_i, \phi_i, T)$ and to the directional hemispherical reflectivity by:

$$a_\lambda(\theta_i, \phi_i, T) = \varepsilon_\lambda(\theta_i, \phi_i, T) \quad \text{Eq. 4}$$

$$a_\lambda(\theta_i, \phi_i, T) = 1 - \int_{2\pi} f_\lambda(\theta_r, \phi_r, \theta_i, \phi_i, T)\, cos\, \theta_r d\Omega_r \quad \text{Eq. 5}$$

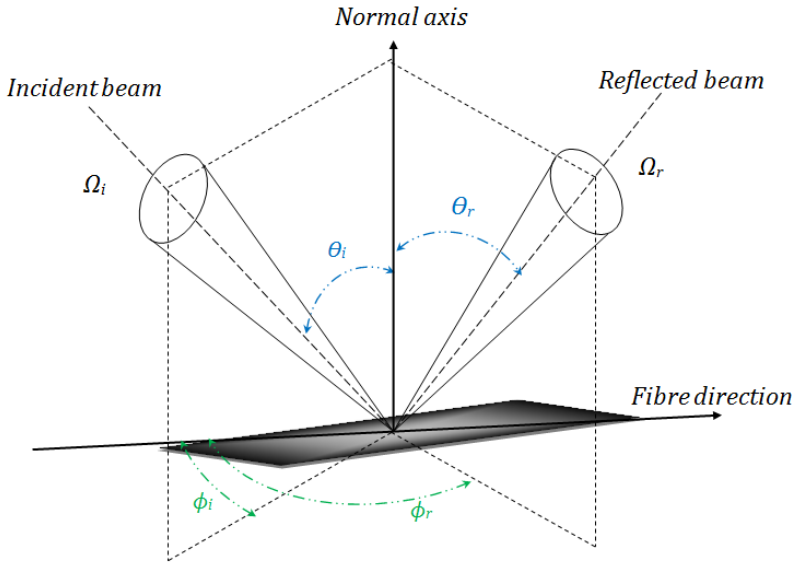

Figure 1: Representation of an incident angle Ω_i and a reflected angle Ω_r on the composite surface. The referential system is chosen with respect to the unidirectional fibres direction.

When the optical response of a material is purely specular, all the reflected flux is located on the *zygomorphic* axis, *i.e* on the axis symmetric to the incident axis with respect to the normal axis, and:

$$\phi_r = \phi_i \quad \text{Eq. 6}$$

For a sake of clarity, let us now define by ρ_{NN} the normal - normal reflectivity given by Eq. 2 when $\theta_i = \theta_r$=0° and $\phi_i = \phi_r = 0°$, and by ρ_{NH} the normal hemispherical reflectivity

*Corresponding author. Email address: benoit.rousseau@univ-nantes.fr

when $\theta_i = 0°$. Moreover, in the following, to lighten the expression of the different notations of the reflectivity, the wavelength will be omitted.

2.2 Experimental developments

2.2.1 Optical units available with the spectrometer

The optical measurements were performed with a Fourier Transform Bruker 80v infrared spectrometer. Different associations of light sources/beamsplitters/detectors can be easily set up on the apparatus so that a spectral range going from the far infrared (80 cm^{-1} - 125 µm) up to visible (22000 cm^{-1} – 0.450 µm) is accessible. Table 1 lists all the possible optical configurations for the acquisition of spectra.

Table 1: Available configurations of light sources/beamsplitters/detectors on the spectrometer Bruker FTIR 80v

	Visible & UV	**NIR**	**MIR**
Spectral range (cm^{-1})	25000 15000	10000 8500	400
Spectral range (µm)	0.4 0.67	1 1.17	25
Light source	Tungsten		Globar
Beam splitters	CaF2	CaF2	KbR
Detectors	RT-Diode Si	RT-INGaAs	RT-DLaTGS

Similarly, the sample units from which measurements are performed are easily switchable. The optical paths allowed by all accessories are represented on Figure 2 for a clear understanding:

- A510/Q-T unit, which gives access to normal - normal specular reflectivity and transmittivity measurements (ρ_{NN} and τ_{NN})[23]. It must be mentioned that, in this unit, the beam is not strictly normal to the surface but slightly shifted (11°) in reason of the optical configuration.
- A652 Teflon and gold coated integration spheres, which allow respectively the measurements of the near and mid infrared hemispherical reflectivity ρ_{NH} and transmittivity τ_{NH} for a normal incidence.
- A513/Q, automated variable angle reflection accessory, which permits to measure the bi-directional reflectivity $\rho(\theta_r, \phi_r, \theta_i, \phi_i, T)$ for $\phi_r = \phi_i$ and, when the

*Corresponding author. Email address: benoit.rousseau@univ-nantes.fr

geometry of illumination is determined [24], to characterize bi-directional reflectivity functions (BDRF) for variable couple of incident and reflected angles (13° to 85°).

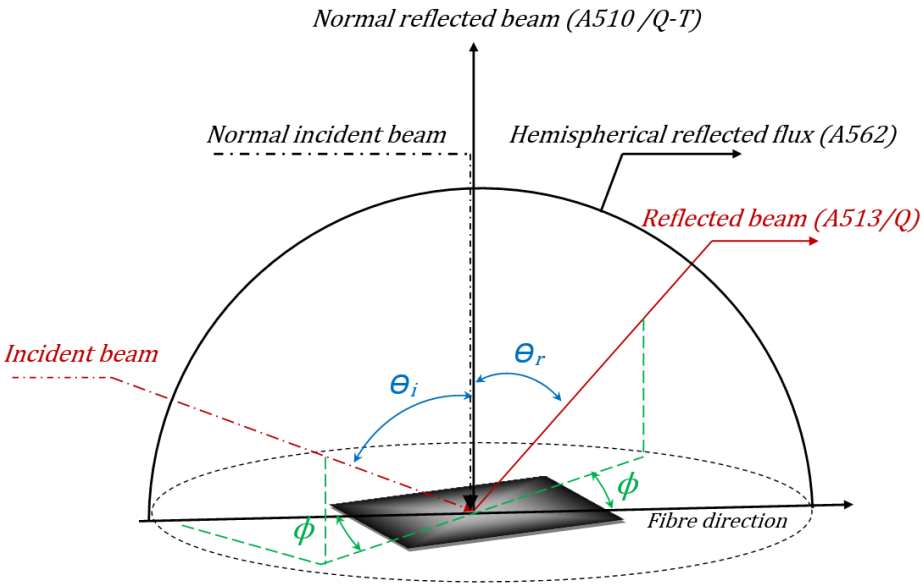

Figure 2: Description of the flux configurations available for a normal incidence (black) with the A510 Q/T and A562 units, and for variable incidence (red) with the A513 unit.

For this last configuration, the references used are respectively an aluminium and a gold mirror for the near-infrared and the mid-infrared range respectively. For the angles outside the specular configurations, a correction Δ must be applied on the reflectivity calculation in order to take into account the fact that the illuminated surface S_i can differ from the surface effectively scanned by the reflection arm S_r:

$$\Delta = \frac{S_i}{S_i \cap S_r} \qquad \text{Eq. 7}$$

Data acquisition can be made at room atmosphere or under primary vacuum (1.82 mbars) for a spectral resolution fixed at 4 cm^{-1}.

2.2.2. Description of the heating compact cell

The heating system is based upon a HFS600 Linkam heating unit (Tadworth, UK) positioned at the location of the one occupied by the sample holder of the A510/Q-T measurement units (Figure 3). The 20 mm diameter central heating block is made of a high thermal conductivity pure silver, so that the final system can reach temperature close to 600°C with an accuracy of 0.1°C and heating rates up to 150°C/min without overshoot.

*Corresponding author. Email address: benoit.rousseau@univ-nantes.fr

In addition, an optional LNP95 freezing system can be used to cool the sample under room temperature down to -196°C, with controlled cooling rates down to -10°C/min.

The 2 mm diameter central hole of the device was widened to 4 mm in order to carry out normal - normal transmittivity measurements in the infrared range with an incident beam sufficiently large to avoid noisy records. The device was mounted on a three axes micrometric guide plate that replaced the previous measurement compartment top. Consequently its position could be selected with 0.1 mm accuracy for the *xyz* directions.

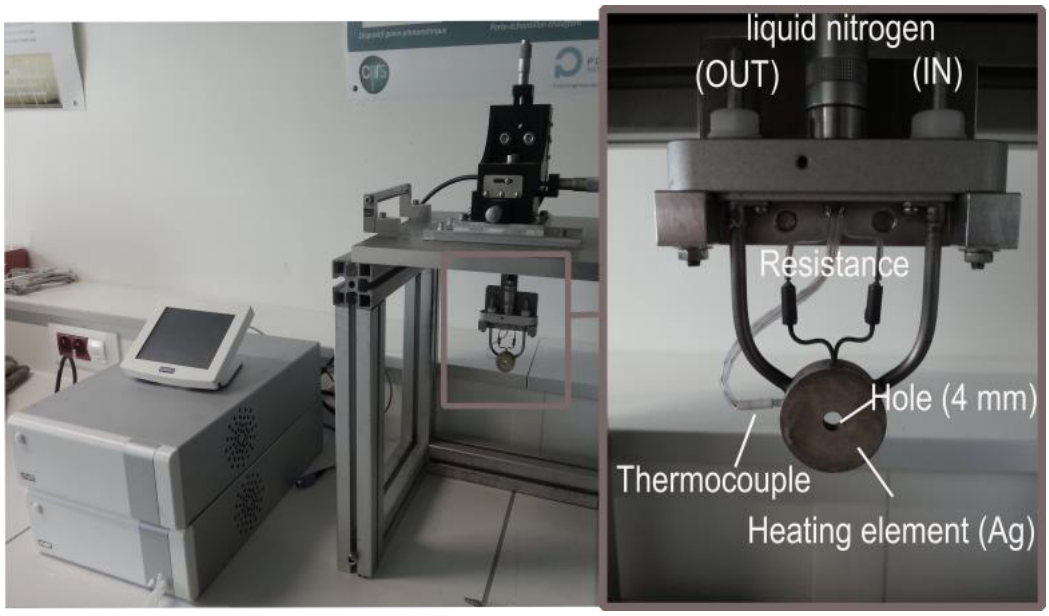

Figure 3: On the left, the heating system held on the three axis unit and its electronic controller; on the right, the heating element Linkam HFS600.

The sample itself is maintained on the surface of the silver element thanks to a MACOR® ceramic insulating shell with a 16 mm diameter aperture at the front and 20 mm diameter at the rear face. If the studied material undergoes phase change (solid to liquid) during the experiment, a protective window must be placed between the sample and the heating element surface. For near infrared measurements, 0.15 mm thick borosilicate glass windows were chosen owing to their high transmitivity in that spectral range (up to 95 %).

2.2.3. Thermal performances of the heating compact cell

The device is controlled by an electronic unit that enables a real-time display of the temperature measured by a thermocouple located as close as possible to the hole. A preliminary calibration was performed using three pure metals with well-known melting

*Corresponding author. Email address: benoit.rousseau@univ-nantes.fr

points: indium (156.6°C), tin (231.9°C) and zinc (419.5°C). Comparing the displayed temperature to actual phase change temperature, the following calibration law was established:

$$T_{displayed}[°C] = -1.36 + 1.027 * T_{actual}[°C] \quad \text{Eq. 8}$$

Besides, the thermal homogeneity of the system was assessed by Infrared thermography using a SC7500 InSb infrared camera equipped with a 50 mm objective of 0.3 mm/pixel spatial resolution. As it can be observed on Figure 4a), the surface of the heating element alone is highly isothermal with a maximal deviation of 0.8 K at an imposed temperature of 100°C. On Figure 4b) the thermographic picture of the complete cell with a borosilicate window placed inside the ceramic sample holder is displayed, and the temperature deviation $T_{max} - T_{min}$ within the illuminated zone, where T_{max} and T_{min} are the maximum and minimum temperatures respectively, is plotted according to the temperature imposed by the electronic controller. For both incident beams with 0.5 mm and 1 mm diameter, the temperature varied linearly (full lines) from 20 to 200°C, and the variations for higher temperature were obtained by extrapolation (dotted lines). The deviation was thus expected to reach 0.5 K for a 0.5 mm diameter beam, and 1.2 K for a 1 mm beam diameter, at 400°C. This confirmed that the developed device fulfilled the requirements to perform accurate radiative measurements at well-controlled temperature.

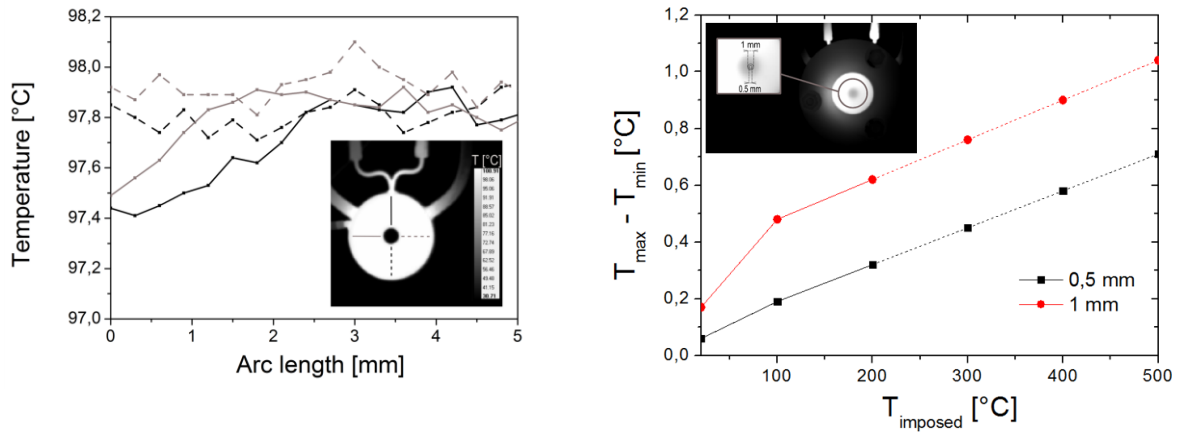

a) b)

Figure 4: a) Infrared thermography measurements on the device alone; the graph represents the temperature probes along the axis with the corresponding colours at 100°C. b) Infrared thermography measurements on the complete system and maximal temperature variation within the illuminated zone.

2.2.4. Validation of the optical performances with reference materials

*Corresponding author. Email address: benoit.rousseau@univ-nantes.fr

The capabilities of the developed heating cell were assessed in the reflection mode for two opaque materials: a thin layer of VO_2:Al deposited on aluminium slab and a gold foil. The samples were held 1 minute at each temperature step before performing a measurement. As can be seen in Table 2 this holding time was much larger than both samples thermal diffusion characteristic time (0.01 s and $9.42e^{-5}$ s for VO_2:Al and gold, respectively) and so ensured that the thermal equilibrium of the illuminated zone was reached.

Table 2: Characteristic diffusion times of the VO2:Al and gold foil samples

Materials	**Diffusivity (s/m^2)**	**Thickness**	**Characteristic diffusion time (s)**	**Isothermal stage time**
Aluminium substrate	1.5e-5	0.4 mm	0.01	1 minute
VO_2 layer	1.2e-4	400 nm	1.24e-9	
Gold foil	1.3e-4	0.11 mm	9.42e-5	1 minute

2.2.4.1. VO_2:Al layer on aluminium slab

An aluminium doped VO_2 400 nm thin film deposited on a 4 mm thick aluminium substrate was elaborated at the Institut Jean Lamour (Nancy, France) by magnetron sputtering [25] deposit process. Vanadium oxide systems are typical thermochromic materials that exhibit an emissivity change at moderate temperature (generally around 68°C), due to a reversible insular to metal transition [26]. The optical properties of the thin film can be tuned by changing the nature of the substrate or by doping the vanadium oxide crystalline structure [27,28].

In the following, the normal reflectivity of the VO_2:Al/Al slab was recorded for a heating/ cooling cycle with temperatures ranging from 20 to 150°C. Since it is an opaque material, the emissivity was deduced using the thermal balance and the Kirchhoff's law (Eq. 4 and Eq. 5). Figure 5 shows the result integrated for wavelengths λ going from 7 up to 14 µm. An emissivity increase around 75°C as well as a hysteresis behaviour between 20 and 150°C can be observed. These evolutions were typical of the semi-conducting to metal transition of the VO_2 [27,29]. This first result shows that the temperature range associated to this evolution for the vanadium oxide is well captured, proving the temperature accuracy of the heating system.

*Corresponding author. Email address: benoit.rousseau@univ-nantes.fr

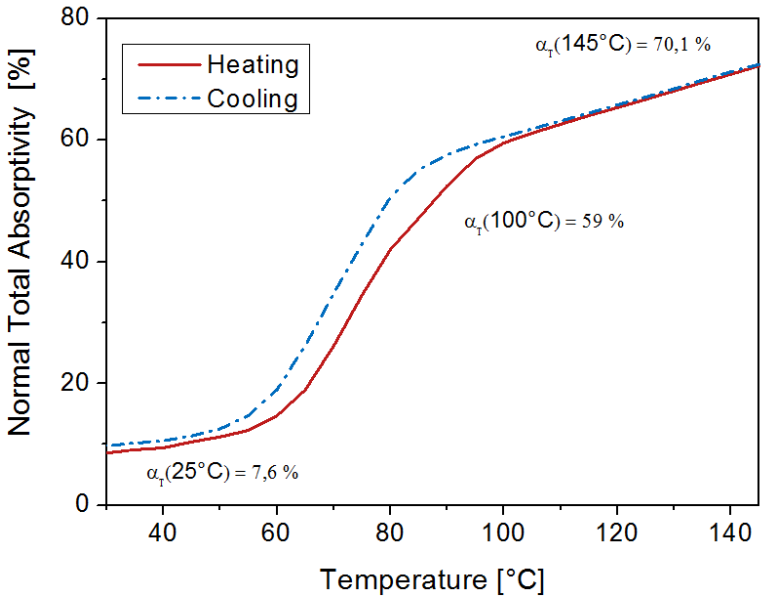

Figure 5: Normal emissivity of the VO_2:Al deposit for a heating from 20 to 150°C, and a cooling, at integrated over the wavelengths λ = 7 to 14 µm.

2.2.4.2. Gold foil

In Ref. [30], Beran *et al* recorded the reflectivity spectra at 25, 300 and 500°C, between λ = 400 and 700 nm, of a 1µm diamond polished pure gold sheet. At λ = 500 nm +/- 20 nm, the reflectivity spectrum was checked to be independent of temperature. This characteristic wavelength, known as the so-called χ-point, at which the emissivity (and so the reflectivity for opaque materials) does not vary with temperature, can be observed in many pure metals [31] and depends on the material only. The levels of reflectivity are controlled by the sample structure (surface aspect, thickness…). Such idiosyncrasy is very useful to test the efficiency of a set-up combining radiative measurements and temperature, as for instance, for pure platinum in [14].

Figure 6 shows the experimental spectral reflectivity (coloured full lines) of the gold foil between λ = 480 and 620 nm, with a resolution of 0.02 nm, recorded for a 1 mm diameter incident beam and for temperatures ranging from 20 to 500°C. The χ-point of invariant emissivity appears clearly at 508 nm and falls in the spectral range found by Beran (grey dashed lines). The normal reflectivity is much lower than the one presented in [30] because of the diffusive behaviour of the foil, that was probably less polished than in the aforementioned study. This point was verified through a surface topography analysis performed with an InfiniteFocus optical profilometer (Alicona, Graz, Austria) that gave

*Corresponding author. Email address: benoit.rousseau@univ-nantes.fr

access to the average root mean square of the height (σ_{RMS}) and to the autocorrelation length (L_c) of the sample. Values of σ_{RMS} = 2.14 µm and Lc = 40.957 µm were obtained over a surface of dimensions 709 * 583 µm^2 with a spatial resolution of 0.1 µm and a magnification *x 20*. Experimental characterization of the bi-directional reflectivity carried out with the A513 /Q automated variable angle reflection accessory shown that weight of the surface scattering is rather high. Indeed this optical feature was checked for θ_i = 13° and $\theta_r \in$ [13, 85°]. By the way, the value of the χ-point in the range going from 20 up to 500°C is for us in good agreement with the one determined in the work of Beran.

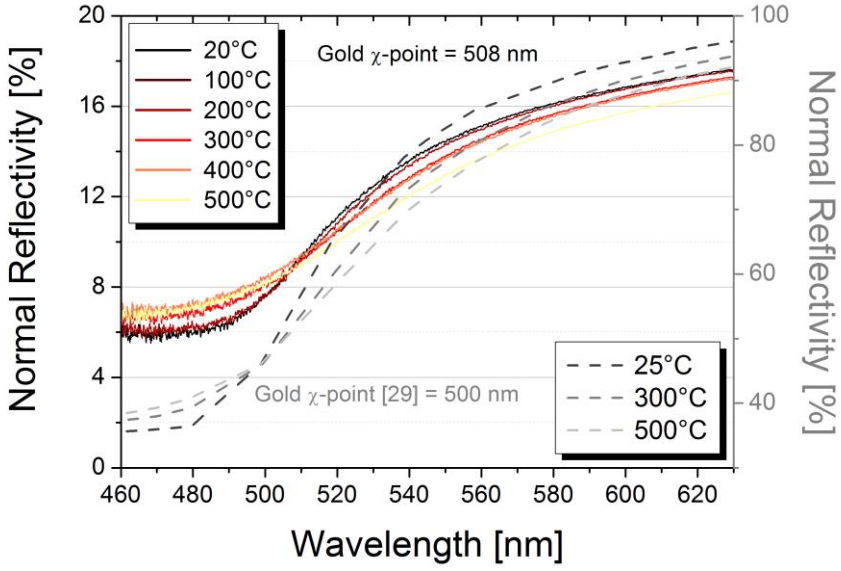

Figure 6 : Reflectivity measurements of a gold foil in the mid infrared range at 20, 100, 200, 300, 400 and 500°C (using the A510/Q-T unit measurement of the spectrometer). In grey, spectra of Ref. [28] are given.

The accuracy of the device on both the wavelength and the temperature was therefore clearly demonstrated thanks to the study of these two reference materials characterized by very different evolutions of their optical properties with temperature. It ensured the ability of the system to detect reflected flux variations and then the robustness of future measurements.

3. Results and discussion

3.1 Material

The studied material is referred to as APC2 and was provided by Cytec Solvay group (Woodland Park, New Jersey, United States). It is composed of a PEEK matrix and of

*Corresponding author. Email address: benoit.rousseau@univ-nantes.fr

55vol% unidirectional carbon fibres. The average thickness of APC2 tapes is about 150 µm. Figure 7 shows a micrograph of the considered tape cut perpendicularly to the fibres direction appearing as white circles on the picture. Their average diameter was about 6.10 µm. A topography analysis performed in the same conditions as before (see §2.2.4.2) allowed to measure an average root mean square of the height σ_{RMS} = 6.048 µm and an autocorrelation length L_c = 40.19 µm. By basing on a previous work performed by Bergstrom et *al.* [32] where surface scattering plots of rough opaque surface were reported according to the ratio σ_{RMS}/L_C, one can predict that the weight of the diffuse scattering will increase in comparison with the homologous smooth surface whatever the angle of incidence.

Besides, the value of σ_{RMS} was very close to the fibre diameter so the apparent surface asperities were mostly due to the carbon fibres present at the surface, all the more so as the few microns thick layer of PEEK matrix at the surface is transparent in that spectral range [400-1500 nm][5].

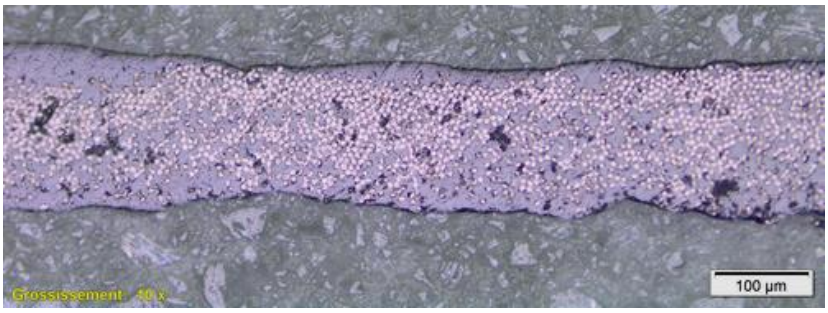

Figure 7: Micrograph of the APC2 tape cut perpendicularly to the fibres direction.

3.2. Sensitivity to the composite surface in normal incidence

The RT-InGaAs detector, which allowed the recording of the reflected intensity associated to the wavelength within the near infrared range was very sensitive and easily blinded. Then, the maximum beam diameter allowed is 1 mm.

A campaign of 25 measurements performed with this accessory at ambient temperature on APC2 samples with orientations $\phi_i = 0°$, 45° and 90° did not outlined any influence of the fibre orientation on the reflectivity. The measurements performed with this unit can then be considered done with a normal incidence despite the 11° incidence (see §2.2.1). However, the surface of the composite is quite irregular under such area as showed on the micrograph (Figure 7). The apparent roughness of the illuminated zone varied

*Corresponding author. Email address: benoit.rousseau@univ-nantes.fr

according to the distribution of fibres influencing directly the measured reflectivity in the visible and near infrared range [400 to 2500 nm]. When averaging over the 25 samples, randomly orientated, the normal reflectivity of the composite was constant over this spectral range and was shown to be:

$$\rho_{NN}(20°C) = (1.75 \pm 0.27)[\%]$$

Similarly, normal - hemispherical measurements where performed on 5 samples with the help of the A562 Teflon unit:

$$\rho_{NH}(20°C) = (8.90 \pm 0.30)[\%]$$

It can be highlighted that the emissivity obtained thanks to Eqs 4 and 5 is high in the infrared range (around 90 %). The emissive power of the material is then important and the heat losses by radiation could become non-negligible in the thermal balance of the AFP process.

3.3. Spectral and bidirectional reflectivity of APC2

Figure 8 shows the spectral bidirectional reflectivities of APC2 measured for wavelengths from 0.6 to 25 µm, with a combination of the RT-InGaas and RT-DLaTGS detectors, for three specular configurations where $\theta_i = \theta_r$ = 15°, 45°, 70° and 75°. For all four cases, small reflexion bands can be observed in the window ranging from 6 up to 14 µm due to optical signature of the carbonaceous skeleton of the PEEK [33]. Thus around 6 µm, one can found the carbonyl stretching vibration with a shoulder at 8 µm and two bands around 11.5 µm. However the intensities of the reflective bands were less important than for pure PEEK as it can be seen in [34]. This effect is due to the presence of carbon fibres characterized by a high absorbing power and reflective spectral behaviours which decrease slowly when wavelengths decline [35] . Also, for the first two orientations (θ_i = 15° and 45°), the levels of reflectivity remained very close, at a low level (around 2.5 %) and almost constant along the whole spectral range. For a grazing incidence of 75° away from the normal axis, the bidirectional reflectivity was higher and increases of around 7 % from 1 to 25 µm. The evolution of the reflectivity level with the beam incidence starts becoming non negligible after a certain angle ($\theta_i \approx 45°$). The amount of absorbed flux at a given wavelength, for instance in AFP processes assisted with 1 µm laser diodes must be calculated in consequence. This graph furthermore shows that the sensitivity to the wavelength is

*Corresponding author. Email address: benoit.rousseau@univ-nantes.fr

small in the range [1 – 6 µm] but become s important above 6 µm. The wavelength should therefore be known precisely when working with such type of IR sources.

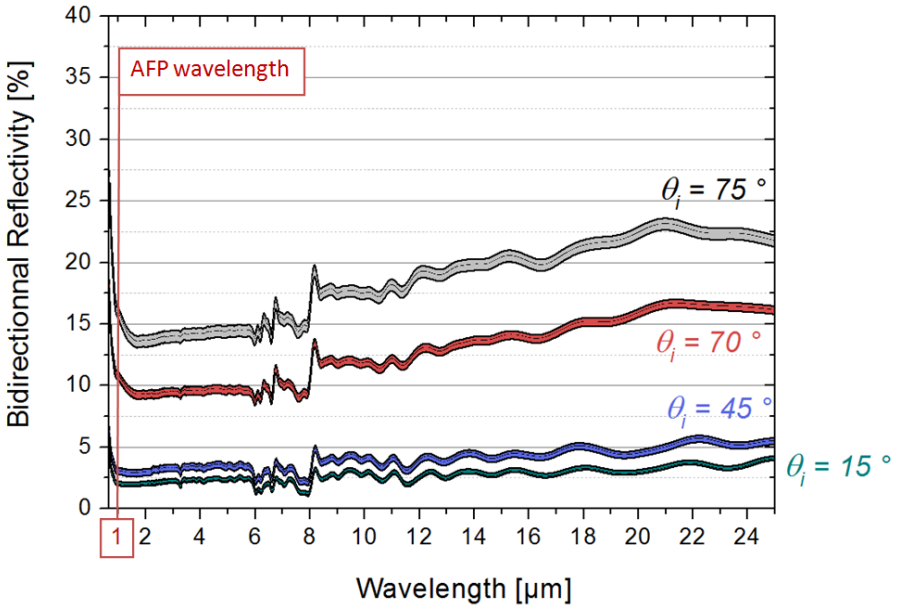

Figure 8 : Bidirectional reflectivity of APC2 from 0.6 to 20 µm, for $\theta_i = \theta_r = 15°, 45°, 70°$ and 75° at T = 20°C and for $\phi_i = 0°$.

While the independency of the reflectivity with the fibre orientation for quasi-normal incidence could be checked (see §3.2), it is expected that for incidence angles farther from the normal axis, the role of the carbon fibres direction with respect to the incident beam becomes more significant [5,8]. Figure 9 represents the distribution of the bidirectional reflectivities at several angles of incidence θ_i and collected along the coplanar axis θ_r, picked at a wavelength of 1 µm and measured for fibre orientations $\phi_i = 0°$, 45° and 90° respectively. As showed above, when $\theta_i = \theta_r$, the bi-directional reflectivity increased as the incidence angle decreased (i.e. towards grazing incidence). But, it also appeared that the reflectivity is maximum, whatever the angle of incidence, when the beam was parallel to the fibre direction ($\phi = 0°$),. In particular, for a given incidence θ_i when $\phi_i = 0°$ the reflectivity reached its maximum on the zygomorphic axis (*i.e* on the axis symmetric to the incident axis with respect to the normal axis). This effect decreased slightly when the unidirectional fibres were rotated away from the plane of illumination ($\phi_i \neq 0°$), until the $\phi_i = 90°$ orientation.

*Corresponding author. Email address: benoit.rousseau@univ-nantes.fr

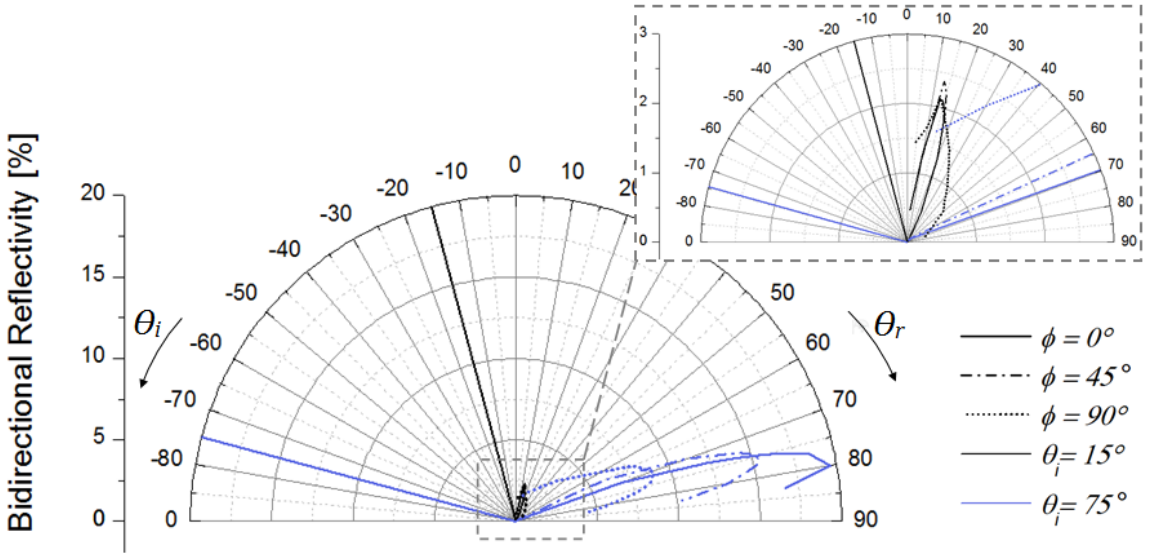

Figure 9: Bidirectional reflectivities of APC2 at λ = 1 µm, 20°C, for fibre / beam orientations $\phi_i = 0°$, $\phi=0°$ (plain), $\phi_i = 45°$ (dashed) and $\phi_i = 90°$ (dotted), and for incident angles θ_i = 15° (black) and θ_i = 75° (blue) (using the A513 /Q unit measurement of the spectrometer).

For each fibre orientation, the reflectivity was integrated over all the reflected angles and the results are presented for two incidences θ_i = 15° (black) and θ_i = 75° (blue) in Figure 10. It must be noted that the considered integrated quantity is not strictly the total value of the reflected flux since the complete hemisphere above the sample surface was not scanned. The angular sector browsed with A513/Q unit collection arm, which degree of liberty was modelled by the black arrows, was compared to the qualitative study performed by Stokes-Griffin [5] in Figure 10 inset. In our measurements, for a perpendicular orientation of the fibres ($\phi_i = 90°$), all the reflected flux is measured. This was confirmed by the fact that the corresponding values were above the results obtained for $\phi_i = 0°$ and $\phi_i = 45°$ where a part of the reflected intensity cannot be captured with the A513/Q unit. Moreover the value of the integrated intensities for an incidence angle of 15° for $\phi_i = 90°$ was equal to 8.5 % that is to say almost equal to the normal hemispherical reflectivity at the same wavelength and measured previously with the A562 Teflon integrating sphere (see §3.2), $\rho_{NH} = 8.9$ %. Finally, all the values were of the same order of magnitude as the directional hemispherical reflectivity at the same wavelength also measured in [5] (red stars data) for increasing angles of incidence. They similarly reached high values of reflected flux for grazing incidence. It is worth noting that

*Corresponding author. Email address: benoit.rousseau@univ-nantes.fr

Stokes-Griffin [5] did not use exactly the same carbon fibre tapes, which can explain the observed gap between their results and ours.

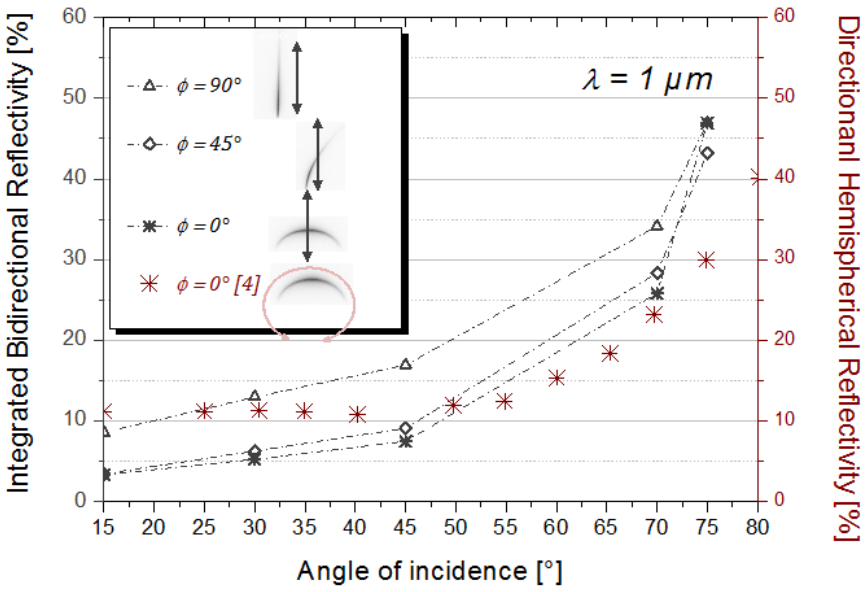

Figure 10: Integrated bidirectional reflectivities (grey lines) for fibre / beam orientations $\phi_i = 0°$ (triangles), $\phi_i = 45°$ (diamonds), and $\phi_i = 90°$ (stars) and comparison with the qualitative profiles presented in [3] (inset). The results of the directional hemispherical reflectivity (red stars) measured in [4] are given for comparison.

The reflection profiles recorded here are typical of the interaction of a beam and a cylinder whose diameter is of the same order of magnitude as the wavelength, indicating that at ambient temperature, the carbon fibres located at the surface control the optical response of the composite sample. The present angular analysis therefore highlights the importance of considering both the incidence and the fibre orientation when working with carbon fibre reinforced materials illuminated by infrared sources.

3.4. Temperature dependence of the normal reflectivity of APC2

The reflected flux of the composite was recorded for temperature ranging from 20°C to 450°C using the developed heating cell mounted on the A510 Q/T unit in the spectrometer. The samples were heated at 100°C/minute between two isothermal steps and held for 30 seconds at the imposed temperature before measurement. As shown in Table 3, the holding time was sufficient to ensure that the association of the protective glass window and the composite material reached the thermal equilibrium.

*Corresponding author. Email address: benoit.rousseau@univ-nantes.fr

Table 3: Characteristic diffusion times for the composite and the borosilicate glass window

Materials	Diffusivity [m^2/s]	Thickness	Characteristic diffusion time [s]	Experimental time
Carbon PEEK	3.2e-7	0.157 mm	0.07	30 seconds
Borosilicate window	6.5e-7	0.17 mm	0.045	

It is first to mention that the material was observed to remain opaque with temperature so the following measurements were performed in the reflection mode only. In practice, the detection mirror of the A510 Q/T unit was maintained in the same reflection position for each series of measurement. Figure 11 shows the normal reflectivity results averaged over 4 series of measurements on different samples for a laser diode wavelength of 980 nm typically used in ATP processes (blue squared symbols).

The reflected flux exhibited a smooth and slight decrease from 1.5 to 1.2 %, when the temperature increased from room temperature up to the melting temperature of the PEEK matrix (343°C). When the temperature was further increased, a fast variation was observed that reached 1.75 % at 400°C. It can be explained by the melting of the semi-crystalline polymer matrix, but this effect is shown to be very small.

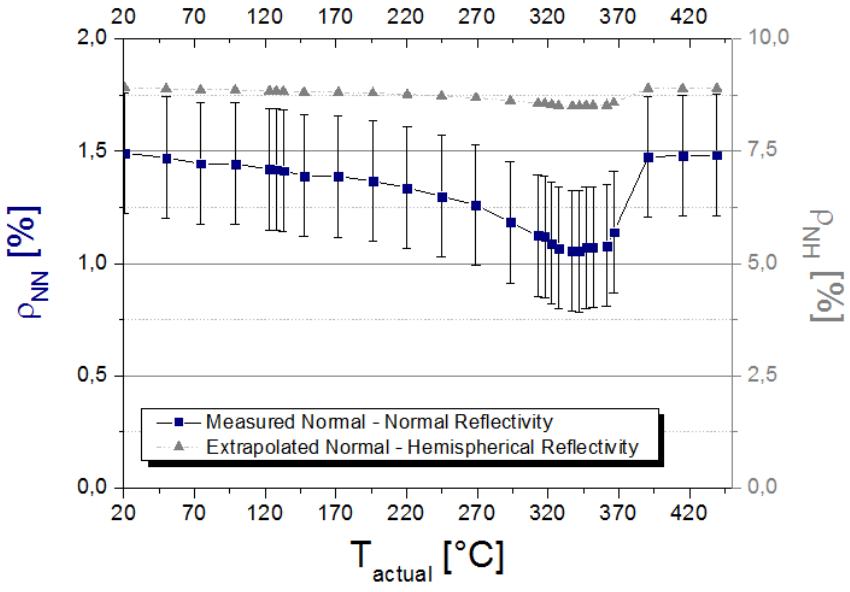

Figure 11: Normal - normal reflectivity of carbon/PEEK composite at 980 nm between 20 and 450°C (using the A510 unit measurement of the spectrometer and the developed heating cell) (coloured lines) and extrapolated normal hemispherical reflectivity (grey lines)

*Corresponding author. Email address: benoit.rousseau@univ-nantes.fr

Although it is known that the PEEK matrix structure can undergo chemical degradation with temperature increase above the PEEK melting point and that this phenomenon is speeded up under oxygen [9,10], in this study, if any degradation of the matrix occurred, it was not obviously captured by the normal reflectivity measurement. That is to say, its influence remained hidden by the scattering of results that can be attributed to the unavoidable material scattering and to the measurement noise. In [6], the authors observe that the presence of a PEEK layer on the top of a carbon fibre tape increases the normal hemispherical reflectivity ρ_{NH} of 2% over 10%, comparing with a layer-less one.

Those results were also consistent with measurements performed by [36] on different carbon based samples, and especially on graphite, between 20 and 600°C. The authors conclude that the temperature rise has no effect on the refractive index of the carbon graphite sample.

The measurements performed in this study on the carbon / PEEK composite imply that neither the chemical evolution of the matrix nor the possible structural changes of the composite assembly with temperature impact the normal – normal reflectivity of the whole material. In [37] the authors have established a relation between the normal hemispherical reflectivity ρ_{NH} and the normal – normal reflectivity ρ_{NN} based on a modified two–fluxes approximation model. For an optically thick material at the thermal equilibrium, ρ_{NH} and ρ_{NN} can be given as a transfer function:

$$\frac{\rho_{NH}(T) - \rho_{NN}(T)}{1 - \rho_{NN}(T)} = f(w_{tr}, \beta) \qquad \text{Eq. 9}$$

Where w_{tr} is the transport albedo and β a constant, both linked to the material structure. At room temperature and at a wavelength of 1 µm we can calculate:

$$\beta(20°C) = 0{,}08099.$$

Thanks to the previous observations, one may assume that the transport term w_{tr} directly linked to the fibrous structure is constant with temperature and may use the following rule of thumb to extrapolate the normal hemispherical reflectivity from ρ_{NN}

$$\rho_{NH}(T) = \rho_{NN} + (1 - \rho_{NN}) * 0.07582 \qquad \text{Eq. 10}$$

*Corresponding author. Email address: benoit.rousseau@univ-nantes.fr

The resulting curve is plotted in light grey on Figure 11 and may presage a similar evolution of the directional hemispherical reflectivity ρ_{DH} with temperature.

Finally, on a modelling point of view, the variations are small enough to deem that the phase change of the matrix does not impact the optical properties of the composite, at least for a normal incidence. In addition to the directional study, the analysis led to the conclusion that in a carbon fibre composite, the material optical response was dominated by the fibres one, whatever the temperature and the angle of incidence.

4. Conclusion

The radiative properties of a carbon fibre thermoplastic composite, commercially known as APC2, was investigated up to 450°C in order to accurately model its thermal behaviour when it is used in industrial forming processes involving radiant sources (laser or infrared lamps). A particular attention was paid to study of the influence of the fibre orientation with respect to the incident beam and to the sample temperature. In order to do so, the spectral dependency of the radiative properties were probed with a Fourier Transform InfraRed spectrometer (Bruker 80v). Commercial (angular and diffuse reflectivity measurement) and homemade accessories directly and easily adapted on the sample compartment of the spectrometer were used. In particular, a high-temperature compact cell was developed and validated on well-known opaque materials in order to measure with a high accuracy, afterwards, the normal/normal reflectivity of the sample up to 450°C.

The results showed that for the carbon fibre thermoplastic composite studied here, there were no significant variations of the normal / normal reflectivity for wavelengths ranging from 0.7 µm to 20 µm, and over a large range of temperature (20-450°C). The directional hemispherical reflectivity according to computation based on the modified two-flux approximation seemed to follow the same trend. Conversely, the room temperature angular study allowed putting forward the active roles played by the beam incident angle and the carbon fibres orientation in the optical properties of the APC2 material. It can be shown that the amount of reflected flux reached its highest level when the fibre orientation was parallel to a grazing laser beam. Furthermore, the adaptation of the heating system for the investigations of the bidirectional reflectivities with temperature

*Corresponding author. Email address: benoit.rousseau@univ-nantes.fr

enabled to confirm the very weak impact of the polymeric matrix on the optical properties of carbon fibres based composites.

Future work will consist in implementing adequate model to extract the optical indices *n* and *k* from the presented reflectivity measurements. These intrinsic parameters are needed to solve the radiative heat balance during industrial processes where the contribution of thermal radiation is dominant such as for the AFP process.

Further developments can also be made to expand the scope of this study to any semi-transparent materials where their radiative properties at moderate temperatures (20-500°C), such as semi-crystalline polymers, are needed.

Acknowledgements

This study is part of the COMPETH project financially supported by IRT Jules Verne (French Institute in Research and Technology in Advanced Manufacturing, Technologies for Composite, Metallic and Hybrid Structures) and the industrial partners of this project; Airbus Group, Airbus Group Innovations, Daher and Solvay.

References

[1] DH-J a. Lukaszewicz, C. Ward C, K.D. Potter, The engineering aspects of automated prepreg layup: History, present and future, Composites Part B Eng 43 (3) (2012) 997 - 1009.

[2] C. Ageorges, Y. Le, Consolidation Mechanisms, In : Fusion Bonding of Polymer Composites, Springer-Verlag London; 2002, p. 105–33.

[3] Z. August, G. Ostander, J. Michasiow, D. Hauber, Recent developments in AFP for thermoplastic composite, SAMPE Journal 50 (2) (2014) 30 -37.

[4] C. M. Stokes-Griffin, P. Compston, A combined optical-thermal model for near-infrared laser heating of thermoplastic composites in an automated tape placement process, Composites Part A Appl Sci Manuf 75 (2014) 104–115.

[5] C.M. Stokes-Griffin, P.Compston, Optical characterisation and modelling for oblique near-infrared laser heating of carbon fibre reinforced thermoplastic composites, Optics and Lasers in Engineering 72 (2015) 1–11.

[6] A. Hohmann, A. Elmaklizi, F. Foschum, F. Voit, F. Bergmann, E. Simon E, et al.

*Corresponding author. Email address: benoit.rousseau@univ-nantes.fr

Optics of carbon fi ber-reinforced plastics – A theoretical and an experimental study, Journal of Quantitative Spectroscopy and Radiative Transfers 180 (2016) 70–76.

[7] S. Grove, Thermal modelling of tape laying with continuous carbon fibre-reinforced thermoplastic, Composites 19 (1988) 367–375.

[8] W. Grouve, Weld strength of laser-assisted tape placed thermoplastic composites, PhD thesis, Universiteit Twente, 2012.

[9] C. Nicodeau, Continuous welding modeling of thermoplastic matrix composites, PhD thesis, Ecole Nationale Supérieure d' Arts et Métiers, Paris, 2005.

[10] P. Patel, T.R. Hull, R.W. McCabe, D. Flath, J. Grasmeder, M. Percy, Mechanism of thermal decomposition of poly(ether ether ketone) (PEEK) from a review of decomposition studies. Polymer Degradation and Stability 95 (2010) 709– 718.

[11] S. Kamba, D. Nuzhnyy, M. Savinov, J. Šebek, J. Petzelt, Infrared and terahertz studies of polar phonons and magnetodielectric effect in multiferroic BiFeO 3 ceramics, Physical Review B 75 (2007)1–7.

[12] F. Gervais, High-Temperature Infrared Reflectivity Spectroscopy by Scanning Interferometry, in: K.J. Button (Ed), Infrared Millimeter Waves V8: Electromagnetic Waves Matter, Academic Press; n.d., 1983, p. 279.

[13] T. Passerat de Silans, I. Maurin I, P. Chaves de Souza Segundo, S. Saltiel, M.-P. Gorza, M. Ducloy, et al., Temperature dependence of the dielectric permittivity of CaF(2), BaF(2) and Al(2)O(3): application to the prediction of a temperature-dependent van der Waals surface interaction exerted onto a neighbouring Cs(8P(3/2)) atom, Journal of Physics and Condensed Matter 21 (2009) 255902 (11p).

[14] D. De Sousa Meneses, P. Melin, L. Del Campo, L. Cosson, P. Echegut, Apparatus for measuring the emittance of materials from far infrared to visible wavelengths in extreme conditions of temperature. Infrared Physics and Technology 69 (2015) 96–101.

[15] L. Del Campo, R.B. Ṕrez-Sáez, X. Esquisabel, I. Fernández, M.J. Tello, New experimental device for infrared spectral directional emissivity measurements in a controlled environment, Review of Scientific Intruments 77 (11) (2006) 113111.

[16] B.D. Demange, M. Bejet, B. Dufour, New Methods for Measuring the Thermal Emissivity of Semi-transparent and Opaque Materials, in Proceedings of the

*Corresponding author. Email address: benoit.rousseau@univ-nantes.fr

Quantitative InfraRed Thermography Conference, Taylor and Francis, Philadelphia, 2006.

[17] Fu T, Duan M, Tang J, Shi C. Measurements of the directional spectral emissivity based on a radiation heating source with alternating spectral distributions. Int J Heat Mass Transf 2015;90:1207–13.

[18] P.J Gero, J.K Taylor, F.A. Best, Fourier Transform Spectrometer for Spectral Emissivity Measurement in the Temperature Range between 60 and n.d., Journal of Physics : Conference Series 13 (2005) 63-66.

[19] M. Honner, P. Honnerová, Survey of emissivity measurement by radiometric methods, Applied Optics, 54 (4) (2015) 669-683.

[20] L.R. Koirala, FTIR-Spectroscopic Measurement of Directional Spectral Emissivities of Microstructured Surfaces, PhD thesis, Helmut Schmidt University of Hamburg, 2004.

[21] L. Li, K. Lu, K. Zhang, Y. Liu, Study of Ti – 6Al – 4V alloy spectral emissivity characteristics during thermal oxidation process, International Journal of Heat and Mass Transfer, 101 (2016) 699–706.

[22] F. Zhang, K. Yu, K. Zhang, Y. Liu, K. Xu, Y. Liu, An emissivity measurement apparatus for near infrared spectrum, Infrared Physics and technology, 73 (2015) 275–280.

[23] A. Simon, G. Zachmann, Automatic beamsplitter exchange unit for a research vacuum FT-IR spectrometer, Vibrational Spectroscopy 60 (2012) 98–101.

[24] R. Baribeau, W.S. Neil, É. Côté, Development of a robot-based gonioreflectometer for spectral BRDF measurement, Journal of Modern Optics 56 (13) (2009) 1497–1503.

[25] D. Mercs, A. Didelot, F. Capon, J. Pierson, A. Pazidis, S. Föste, et al, Innovative smart selective coating to avoid overheating in highly efficient thermal solar collectors, Energy Procedia 91 (2016) 84–93.

[26] M. Soltani, A.B. Kaye, Properties and Applications of Thermochromic Vanadium Dioxide Smart Coatings, In book: Intelligent Coatings for Corrosion Control, pp.461-490, Elsevier Inc, 2015.

[27] M. Benkahoul, M. Chaker, J. Margot, E. Haddad, R. Kruzelecky, B. Wong, et al., Thermochromic VO2 film deopsited on Al with tunable thermal emissivity for space applications, Solar Energy Materials and Solar Cells 95 (2011) 3504–3508.

*Corresponding author. Email address: benoit.rousseau@univ-nantes.fr

[28] V. Théry, J.-C. Orlianges, A. Boulle, A. Mennai, A. Bessaudou, F. Cosset, A. Beaumont, Strain and thickness dependence of the metal-insulator transition n VO2 epitaxial films, Proceeding in Europen Material Research Society, Spring Meet, 2015.

[29] H. Prod'homme, J. Ordonez-Miranda, Y. Ezzahri, J. Drevillon, K. Joulain, Optimized thermal amplification in a radiative transistor, Journal of Applied Physics, 199 (2016) 1–6.

[30] A. Beran, The Reflectance Behaviour of Gold at Temperatures up to 500°C. TMPM Tschermaks Min Petr Mitt 1 34 (1985) 211–215.

[31] R. Gilblas, T. Sentenac, Y. Le Maoult,D.De, Thermographie monochromatique exploitant l' invariance de l' émissivité avec la température, Congrès la Société Française Thermique, Toulouse, 2016.

[32] D. Bergstrom, J. Powell, A. Kaplan, A ray-tracing analysis of the absorption of light by smooth and rough metal surfaces, Journal of Applied Physics 101 (2007) 113504/1-11.

[33] H.X. Nguyen, H. Ishida, Molecular analysis of the melting behaviour of poly (aryl-ether-ether-ketone) 27 (1986) 1400–1405.

[34] J.M. Chalmers, N.J. Everall SE. Specular Reflectance : A Convenient Tool for Polymer Characterisation by FTIR-Microscopy ?, Micron 27 (1996) 315–328.

[35] P.J. Foster, C.R. Howarth, Optical constants of carbons and coals in the infrared, Carbon, 6 (5) (1968) 719–724.

[36] B.J. Stagg, T.T Charalampopoulos, Refractive indices of pyrolytic graphite, amorphous carbon, and flame soot in the temperature range 25° to 600°C, Combustion Flame 94 (1993) 381–396.

[37] L.A. Dombrovsky, I. National, A. Ly, A. De, Modified two-flux approximation for identification of radiative properties of absorbing and scattering media from directional-hemispheric, Journal of the Optical Society of America 23 (1) (2006) 91-98.

*Corresponding author. Email address: benoit.rousseau@univ-nantes.fr